Supercurrent Detection of Topologically Trivial Zero-Energy States in Nanowire Junctions

Oladunjoye A. Awoga, Jorge Cayao,* and Annica M. Black-Schaffer
Department of Physics and Astronomy, Uppsala University, Box 516, S-751 20 Uppsala, Sweden

(Received 8 April 2019; published 12 September 2019)

We report the emergence of zero-energy states in the trivial phase of a short nanowire junction with a strong spin-orbit coupling and magnetic field, formed by strong coupling between the nanowire and two superconductors. The zero-energy states appear in the junction when the superconductors induce a large energy shift in the nanowire, such that the junction naturally forms a quantum dot, a process that is highly tunable by the superconductor width. Most importantly, we demonstrate that the zero-energy states produce a π shift in the phase-biased supercurrent, which can be used as a simple tool for their unambiguous detection, ruling out any Majorana-like interpretation.

DOI: 10.1103/PhysRevLett.123.117001

Majorana bound states (MBSs) in topological superconductors have generated remarkable interest due to their potential applications in fault tolerant quantum computation [1–3]. A promising route for engineering the topological phase is based on nanowires (NWs) with strong Rashba spin-orbit coupling (SOC) and proximity-induced s-wave superconductivity, with MBSs emerging at the NW ends for sufficiently large magnetic fields [4–6]. Initial issues, such as a soft superconducting gap [7–13] of the first experiments [14–19], have been resolved through the fabrication of high-quality interfaces between the NW and external superconductors (SCs) [20–30].

Despite the advances, there is still no consensus whether or not MBSs have been observed. In fact, recent reports show that trivial zero-energy Andreev bound states (ABSs) from, e.g., chemical potential inhomogeneities, appearing well outside the topological phase [31–34], can also lead to a $2e^2/h$ quantized conductance [35,36], a feature previously attributed solely to MBSs [37]. This controversy can at least partially be attributed to oversimplified models used to describe the experiments. Indeed, a common treatment of superconductivity has been to simply add an induced superconducting gap into a one-dimensional (1D) NW model, ignoring all other effects caused by coupling a SC to a NW.

A more accurate approach is to study the whole NW + SC system, since the achieved high-quality interfaces result in a strong coupling between NW and SC and thus the SC generates both an induced gap and affect other NW parameters. Importantly, the NW energies are shifted when the coupling between the SC and NW is strong due to the lowest states having a large weight in the SC [38–42]. This results in an effective chemical potential μ_{eff} in the NW, which regulates when the NW reaches the topological phase. Therefore, using a NW + SC model is crucial for gaining further insights into the experimental situation.

In this Letter, we study the whole NW + SC system and find trivial zero-energy ABSs spontaneously emerging in a NW strongly coupled to two SCs forming a short superconductor-normal-metal-superconductor (*S-N-S*) junction. The zero-energy ABSs appear in the junction when the SCs induce a large μ_{eff} in the NW, such that the junction forms natural quantum dot (QD). The QD formation occurs at regular intervals, every Fermi wavelength increment in SC width, and is thus predictable. By simply regulating the width of the SCs, we can tune the NW from an ideal regime with no energy shifts, to forming a QD or even a potential barrier (PB) at the junction. The formation of the QD and its zero-energy ABSs is therefore very different from previous situations where the QD was simply put in by hand [36,43–48]. Most importantly, we find that the trivial zero-energy QD states produce a π shift in the phase-biased supercurrent, while MBSs appearing in the topological phase do not. Thus, the Josephson effect in short *S-N-S* junctions offers a remarkably powerful, yet simple tool for distinguishing between trivial zero-energy states and MBSs.

Model.—We use a 1D NW with strong SOC with the right (R) and left (L) parts strongly coupled to the middle of two 2D conventional SCs, leaving only the central part of the NW uncoupled and forming a short *S-N-S* junction, see Fig. 1(a). By varying a magnetic field parallel to the NW we easily tune the topology of the junction. The Hamiltonian is thus $\mathcal{H} = \mathcal{H}_{\text{NW}} + \mathcal{H}^{L}_{\text{SC}} + \mathcal{H}^{R}_{\text{SC}} + \mathcal{H}_{S-W}$, with

$$\mathcal{H}_{\mathrm{NW}} = \sum_{x=1,\sigma\sigma'}^{L_{\mathrm{NW}}} d^{\dagger}_{x\sigma}(\varepsilon_{\mathrm{NW}}\delta_{\sigma\sigma'} + B\sigma^{x}_{\sigma\sigma'})d_{x\sigma'} - \sum_{x=1,\sigma}^{L_{\mathrm{NW}}-1} d^{\dagger}_{x\sigma}(t_{\mathrm{NW}}\delta_{\sigma\sigma'} - i\alpha_{\mathrm{NW}}\sigma^{y}_{\sigma\sigma'})d_{x+1,\sigma'} + \mathrm{H.c.},$$

$$\mathcal{H}^{R/L}_{\mathrm{SC}} = \sum_{i,j,\sigma} c^{\dagger}_{i\sigma}[(\varepsilon_{\mathrm{sc}}\delta_{ij} - t_{\mathrm{sc}}\delta_{\langle i,j\rangle})c_{j\sigma} + \Delta^{R/L}_{\mathrm{sc}}(i)c^{\dagger}_{i\uparrow}c^{\dagger}_{i\downarrow}] + \mathrm{H.c.},$$

$$\mathcal{H}_{S-W} = -\Gamma\sum_{\mathrm{i}}\sum_{x=1,\sigma}^{L_{\mathrm{NW}}} c^{\dagger}_{\mathrm{i}\sigma}d_{x\sigma}\delta_{i_y,\frac{L_y+1}{2}}\delta_{i_x,x} + \mathrm{H.c.},$$

where $d_{x\sigma}$ is the destruction operator for a particle with spin σ at site x in the L_{NW} long NW, while $c_{i\sigma}$ is the destruction operator at site $i = (i_x, i_y)$ in the 2D SCs with length L_x, width L_y. Here, $\langle\cdots\rangle$ implies nearest neighbor sites, t represents the nearest neighbor hopping, and μ the chemical potential, such that the on-site energies $\varepsilon_{\mathrm{NW}} = 2t_{\mathrm{NW}} - \mu_{\mathrm{NW}}$, $\varepsilon_{\mathrm{sc}} = 4t_{\mathrm{sc}} - \mu_{\mathrm{sc}}$. In the NW $\alpha_{\mathrm{NW}} = \alpha_R/2a$ is the SOC, with α_R the SOC strength and a the lattice constant, and B is the effective Zeeman coupling caused by the magnetic field with σ^{ν} a Pauli matrix. The SCs have an on-site s-wave superconducting order parameter $\Delta^{R/L}_{\mathrm{sc}}(i) = |\Delta_{\mathrm{sc}}|e^{i\phi_{R/L}}$, with $\phi_{R/L}$ being the SC phase. Finally, $\mathcal{H}_{S-W}$ is the NW-SC tunneling Hamiltonian with finite coupling strength Γ, whenever the NW touches either SCs.

We solve the Hamiltonian within the Bogoliubov–de Gennes framework [49] using parameters in units of t_{sc}: $\mu_{\mathrm{sc}} = 0.5$, $\mu_{\mathrm{NW}} = 0.02t_{\mathrm{NW}}$, $\alpha_{\mathrm{NW}} = 0.05t_{\mathrm{NW}}$, $t_{\mathrm{NW}} = 4$, which accounts for the small NW effective mass and mismatching Fermi wave vectors in NW and SC, and being close to realistic values. We also set $\Delta_{\mathrm{sc}}(i) = 0.1$, $\phi_R = 0$, and $\phi_L = \phi$. Here, the strong coupling regime, with the induced gap in the NW close to Δ_{sc}, is reached around $\Gamma = 0.7$. For smaller Δ_{sc} and μ_{sc}, a smaller Γ achieves strong coupling. Further, we use $L_x = 520a$, $L_{\mathrm{NW}} = 1000a$, and keep the N junction $2a$ long, to reach realistic sizes with the outer ends of the NWs well within the SCs. The width of the SC, L_y, is varied in order to tune the influence of the SC on the NW [39–42]. We have verified that our results remain qualitatively unchanged for Δ_{sc} and Γ both being smaller (or even larger), as well as when $\Delta_{\mathrm{sc}}(i)$ is calculated self-consistently [50–54]. Our results also do not depend on L_x, L_{NW}, junction length, provided L_x, L_{NW} are longer than the superconducting coherence length and the junction is short; see Supplemental Material (SM) for more information [55].

As a result of strong coupling to the SC, all inherent NW parameters are renormalized [38–42,56]. Most important is an energy shift of the NW bands [42]. We encode this by an effective chemical potential μ_{eff}, which we define as the energy of the bottom of the hybridized subband closest to the Fermi energy (since superconductivity occurs around the Fermi energy). We extract μ_{eff} deep in the S regions of the NW and find that it oscillates as a function of L_y, see Fig. 1(b). The oscillations are due to a mismatch between the SC and NW bands, with the period (here $8a$) given by the SC Fermi wavelength. Thus, by changing L_y we can easily tune through a range of μ_{eff}.

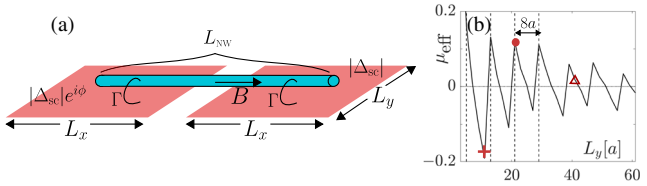

FIG. 1. (a) 1D NW (cyan) coupled to the middle of two 2D SCs (red) by Γ. A short central region of the NW is left uncoupled, giving a short S-N-S junction with a ϕ superconducting phase difference. (b) Effective chemical potential profile deep into the S parts of the NW as a function of SC width L_y. Markers are representative points at which three cases are studied: ideal (triangle), PB (cross), and QD (dot).

Low-energy spectrum.—When the S regions of the NW get a nonzero μ_{eff}, the properties of the S-N-S junction change. We show this first by studying the Zeeman dependent low-energy spectrum at $\phi = 0$ for three values of the SC width L_y, see Figs. 2(a)–2(c). The common characteristic in all three cases is that the spectrum exhibits a sizable gap at zero B, indicating the presence of superconductivity, which then closes and reopens at the critical field B_c signaling the topological phase transition (green dashed line). By calculating the topological invariant for a NW coupled to a single SC [57] we verify that the gap closure in Figs. 2(a)–2(c) matches the topological phase transition point. In the topological phase the S-N-S system hosts a pair of MBSs, with zero energy, one at each end of the NW (outer MBS), for all cases. Since μ_{eff} changes the NW properties, we find that B_c also changes somewhat with L_y.

Remarkably, there is a very strong effect of L_y on the low-energy spectrum inside the junction, resulting in the emergence of additional low-energy states below B_c. These can be understood when comparing μ_{eff} in the S regions of the NW to the native chemical potential μ_{NW}, which is still the relevant energy in the N region. In fact, in Fig. 2(a) the low-energy spectrum does not exhibit any unusual features, since here $\mu_{\mathrm{eff}} \approx \mu_{\mathrm{NW}}$ [triangle in Fig. 1(b)]. We refer to this regime as the ideal case. However, when $\mu_{\mathrm{eff}} < \mu_{\mathrm{NW}}$ [cross in Fig. 1(b)], the junction acts as a potential barrier (PB) and we see in Fig. 2(b) that such a PB junction can host discrete low-energy levels in the trivial phase. Finally, when $\mu_{\mathrm{eff}} > \mu_{\mathrm{NW}}$ [dot in Fig. 1(b)], there is instead a quantum dot (QD) profile in the junction. Remarkably, this QD accommodates a clear single zero-energy crossing in the trivial phase, see Fig. 2(c).

We here stress that the QD with a zero-energy crossing in the trivial phase emerges spontaneously at the junction, just due to strong NW-SC coupling and tuning L_y. We have

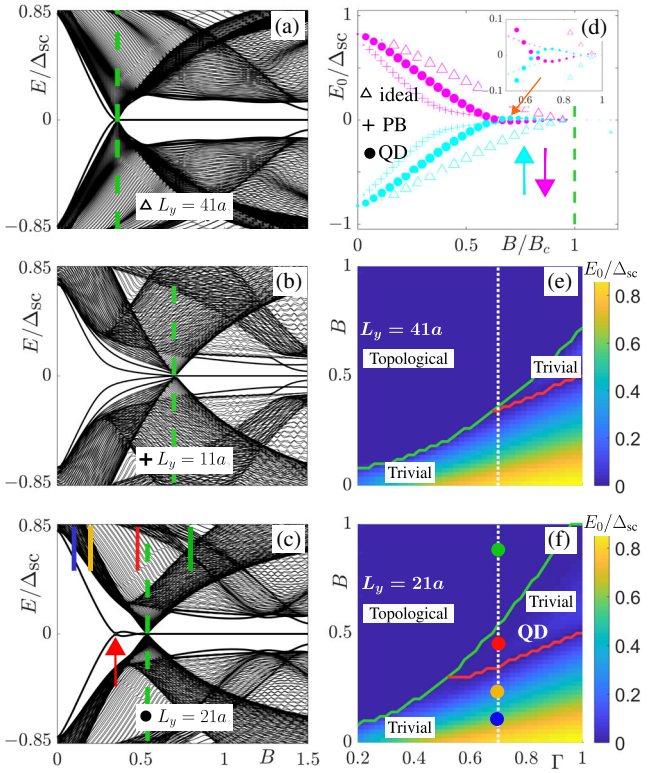

FIG. 2. Zeeman field-dependent spectrum at $\phi = 0$ for ideal ($L_y = 41a$) (a), PB ($L_y = 11a$) (b), and QD ($L_y = 21a$) (c) cases. Vertical dashed green lines in (a)–(d) mark the topological phase transition, while the red arrow in (c) marks the start of zero-energy levels. (d) Local spin projection at the junction $S^{(x)}_{x=L_{NW}/2}$ in the lowest level E_0 for cases (a)–(c) as a function of B/B_c. Cyan (magenta) marks spin up (down) while marker size denotes magnitude. (e),(f) Color plot of E_0 as a function of Γ and B for $L_y = 41a$ (e) and $L_y = 21a$ (f) cases. The green line marks the topological phase transition, the red line marks the start of the supercurrent π shift, and the dotted white line marks $\Gamma = 0.7$. The filled circles in (f) denote colored markings in (c).

numerically verified that the QD zero-energy states occur for $\tilde{\alpha} < B < B_c$, where $\tilde{\alpha}$ is the renormalized SOC in the NW (dependent on L_y and Γ, here $\tilde{\alpha} \approx 0.5\alpha_{NW}$), see SM [55]. Zero-energy states have previously been reported in simple 1D models with a QD put in by hand [32,36,44,47,48,58], producing signatures similar to MBSs and thus challenging attempts trying to distinguish between such trivial zero-energy levels and MBSs [36,42,59,60]. In our work the QD instead develops naturally and we also find that the trivial zero-energy crossings appear solely in the QD regime, not in the PB or ideal regimes.

Further insights can be obtained from the local spin projection along B (i.e., the x component), in the lowest level E_0 states, which is given by $S^{(x)}_x = v^*_{x\uparrow}u_{x\downarrow} + u^*_{x\downarrow}v_{x\uparrow}$, and the superscript (subscript) denotes the component (position) and $u_{x\sigma}$, $v_{x\sigma}$ are the wave function amplitudes at position x [61–64]. In Fig. 2(d) we show $S^{(x)}_x$ at the junction, i.e., $x = L_{NW}/2$, with marker size denoting the magnitude. $S^{(x)}_{L_{NW}/2}$ vanishes in the topological phase as the lowest level E_0 is then the outer MBSs. However, in the trivial phase the zero-energy crossing in the QD case is accompanied by an exchange of spins in the occupied state. Such spin exchange does not occur in the other cases, leading to a fundamental difference in the spin properties of the QD and PB cases, even if they both host discrete low-energy states below the quasicontinuum.

We finally analyze the size of the regime where trivial zero-energy QD states are observed. In Figs. 2(e) and 2(f) we plot E_0 as a function of Γ and B for the cases in Figs. 2(a) and 2(c), respectively. From the low-energy spectrum, we identify the topological phase transition (green line) and the beginning of the zero-energy state QD regime (red line). The QD regime forms a triangular region which is clearly enlarged with Γ. Remarkably, Fig. 2(e) shows that even wide SCs can host a QD regime with trivial zero-energy states for strong enough couplings [white dotted line marks $\Gamma = 0.7$ from the ideal case in Fig. 2(a)]. We thus conclude that *S-N-S* junctions readily form natural QDs hosting trivial zero-energy states in the strong coupling regime.

Phase dependence.—Next, we allow for a finite phase ϕ across the *S-N-S* junction. In particular, we study the phase-dependent energy spectrum for the QD case in Fig. 2(c) at the B values identified by the colored bars. At very low B (blue) we find ABSs detached from the quasicontinuum and exhibiting the usual cosine behavior [65,66], see Fig. 3(a). These lowest energy states are localized at the junction for both $\phi = 0, \pi$, see blue line in Figs. 3(e) and 3(f). On the other hand, in the topological phase at very large B (green) four MBSs appear in the system: two dispersionless outer MBSs and at $\phi = \pi$ also two MBSs located in the junction (inner MBSs), see Fig. 3(d) for the energy spectrum and Figs. 3(e) and 3(f) for the wave function probabilities. In both the low B trivial and high B topological regimes, the lowest level reaches maximum negative energy at $\phi = 0$. The *S-N-S* junction is therefore in the 0 state because the free energy, $F = \sum_{n<0} E_n$, is minimized at $\phi = 0$, see blue and green lines in the inset of Fig. 3(a).

It is at intermediate B in the trivial phase that dramatic changes takes place. First, the ABSs move towards zero energy with increasing B and start to cross, see Fig. 3(b). As a consequence, the free energy, plotted in gold in the inset in Fig. 3(a), has a global minimum at $\phi = 0$ and a local minimum at $\phi = \pi$. The junction is thus in a $0'$ state [67]. Further increasing B we find that the global and local minima interchanges, eventually reaching the situation in Fig. 3(c). Here, the zero-energy crossing is at $\phi = 0$, implying that a full π shift has occurred in the low-energy spectrum. As a consequence, this junction is in a π state, since the minimum of F is now at $\phi = \pi$, see red Fig. 3(a) inset. At $\phi = 0$ the ABSs are localized at the junction, as in

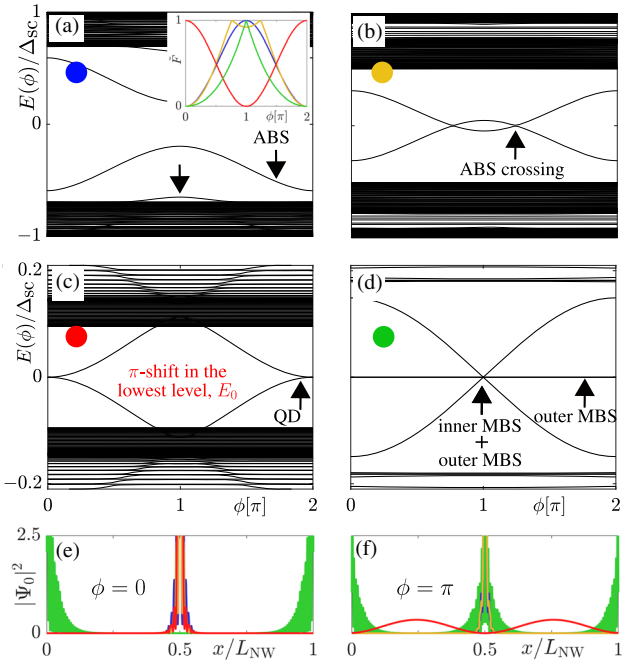

FIG. 3. (a)–(d) Phase-dependent low-energy spectrum in the QD case ($L_y = 21a$), obtained at the color-marked B values in Fig. 2(c). Inset in (a): scaled free energy $\tilde{F} = (F - F_{min})/(F_{max} - F_{min})$ for (a)–(d), with $F_{min\ (max)}$ the minimum (maximum) of F in each case. Probability density of the lowest state, $|\Psi_0|^2 \times 10^3$, in (a)–(d) at $\phi = 0$ (e) and $\phi = \pi$ (f).

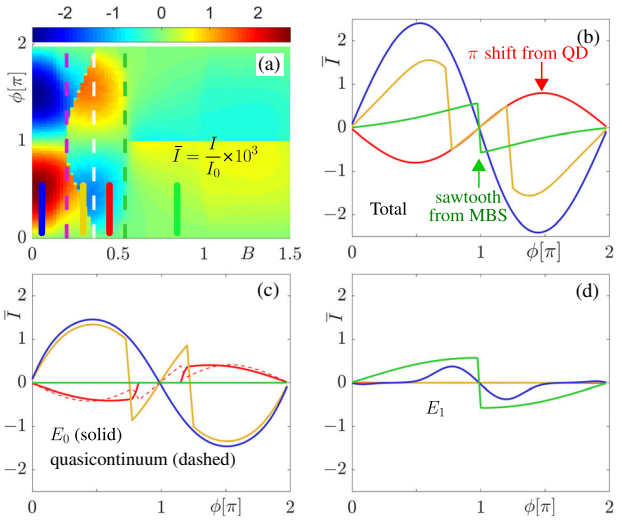

FIG. 4. (a) Color plot of the supercurrent for the QD case ($L_y = 21a$) as a function of ϕ and B. Topological phase transition (green dashed line), beginning of ABS crossings in phase-dependent energy spectrum (magenta), and zero-energy crossing at $\phi = 0$, i.e., the red arrow in Fig. 2(c) (white). Total supercurrent (b), with contributions from E_0 (c) and E_1 (d) energy levels at the color-marked B values Fig. 2(c), repeated in (a).

all other cases in the trivial phase, while at $\phi = \pi$ the lowest energy state is completely delocalized because of mixing with the quasicontinuum, see red in Figs. 3(e) and 3(f).

We find that the π state always emerges when the *S-N-S* junction hosts a pair of QD states with zero-energy crossings. In essence this is because the QD forces the ABS to be at or close to zero energy for $\phi = 0$. We also note that the QD introduces a phase dependence for the quasicontinuum, unlike in conventional short junctions [68]. We have also verified that the ideal and PB cases do not exhibit any π states, see SM [55]. Thus, the phase-dependent energy spectrum offers a remarkably clear differentiation between topologically trivial zero-energy QD levels and MBSs.

Current-phase relationship.—To perform a direct detection of the QD trivial zero-energy states we consider the junction supercurrent $I(\phi)$, obtained from $I(\phi) = I_0(\partial F/\partial\phi)$, where $I_0 = e/\hbar$. Figure 4(a) shows a color plot of $\bar{I} = I(\phi)/I_0$ as a function of ϕ and B for the QD case in Fig. 2(c). For a complete understanding of how the QD levels contribute to $I(\phi)$, we also plot both the total supercurrent and the contributions from the lowest (E_0) and first excited (E_1) energy levels in Figs. 4(b), 4(c) and 4(d), respectively, for the same B values analyzed in Fig. 3.

At low B in the trivial phase $I(\phi)$ displays the usual $\sin(\phi)$-like behavior. This is the 0 state, where E_0 gives the dominating contribution to the supercurrent, albeit E_1 also gives a small positive contribution; see blue line in Figs. 4(b)–4(d). Beyond the topological phase transition (green dashed line) the situation is also easy to understand. Here, $I(\phi)$ has a characteristic sawtooth profile at $\phi = \pi$ due to the special zero-energy behavior of the inner MBS at $\phi = \pi$, which has been proposed as a signature of true MBSs in short *S-N-S* junctions [65,66].

Between the magenta and white lines in Fig. 4(a), we find a region with a discontinuous $I(\phi)$, which is caused by the ABS crossings in Fig. 3(b). Here, the E_0 levels are strongly dispersive with ϕ leading to the largest contributions to $I(\phi)$, see gold in Fig. 4(c). Finally, between the dashed white and green lines in Fig. 4(a), we find a full sign reversal for the supercurrent, with the white line corresponding to the red arrow in Fig. 2(c) indicating the zero-energy crossing at $\phi = 0$. This π-shifted supercurrent arises from the special behavior of the low-energy spectrum: the lowest ABSs exhibit maximum energy at $\phi = \pi$, see Fig. 3(c), instead of a minimum as is the case for conventional junctions [68]. Thus, the E_0 level contributes strongly to the π-shifted supercurrent, as also seen in red in Fig. 4(c). Because of the presence of the QD levels, the quasicontinuum also gives a π-shifted contribution to $I(\phi)$. For the ideal and PB junctions, the ABS energy spectrum only exhibits 0, 0′, π' states, but never the π state and thus we never see a π-shifted supercurrent. Some signatures of the QD and PB junctions can also be captured by the critical current but not as clear as the π shift, see SM [55].

For *S-N-S* junctions with trivial zero-energy crossings we always find a π-shifted supercurrent, independent on any zero-energy pinning after the crossing. These zero-energy levels, appearing in the QD regime, are, however, somewhat

sensitive to SOC [44], with very large SOC inducing level repulsion, which gaps the spectrum and thus destroys the supercurrent π shift, see SM [55]. Interestingly, QD levels in clearly nontopological Josephson junctions have previously been shown to change the state of the junction from 0 to π with increasing magnetic field and also associated with a spin exchange [19,67,69–75], fully consistent with our findings.

In conclusion, we demonstrate the emergence of zero-energy states in the trivial phase of short *S-N-S* NW junctions, due to strong NW-SC coupling causing a QD formation in the NW and tunable by the SC width. Most significantly, these zero-energy states produce a π shift in the phase-biased supercurrent, making them easily distinguishable from MBSs appearing in the topological phase.

We thank C. Reeg and C. Schrade for useful discussions and M. Mashkoori for helpful comments on the manuscript. We acknowledge financial support from the Swedish Research Council (Vetenskaprådet), the Göran Gustafsson Foundation, the Swedish Foundation for Strategic Research (SSF), the Knut and Alice Wallenberg Foundation through the Wallenberg Academy Fellows program, and the EU-COST Action CA-16218 Nanocohybri. Simulations were performed on resources provided by the Swedish National Infrastructure for Computing (SNIC) at the Uppsala Multidisciplinary Center for Advanced Computational Science (UPPMAX).

*jorge.cayao@physics.uu.se

[1] A. Y. Kitaev, Unpaired Majorana fermions in quantum wires, Phys. Usp. **44**, 131 (2001).
[2] C. Nayak, S. H. Simon, A. Stern, M. Freedman, and S. Das Sarma, Non-abelian anyons and topological quantum computation, Rev. Mod. Phys. **80**, 1083 (2008).
[3] C. Schrade and L. Fu, Majorana Superconducting Qubit, Phys. Rev. Lett. **121**, 267002 (2018).
[4] R. M. Lutchyn, J. D. Sau, and S. Das Sarma, Majorana Fermions and a Topological Phase Transition in Semiconductor-Superconductor Heterostructures, Phys. Rev. Lett. **105**, 077001 (2010).
[5] Y. Oreg, G. Refael, and F. von Oppen, Helical Liquids and Majorana Bound States in Quantum Wires, Phys. Rev. Lett. **105**, 177002 (2010).
[6] J. Alicea, Majorana fermions in a tunable semiconductor device, Phys. Rev. B **81**, 125318 (2010).
[7] E. J. H. Lee, X. Jiang, R. Aguado, G. Katsaros, C. M. Lieber, and S. De Franceschi, Zero-Bias Anomaly in a Nanowire Quantum Dot Coupled to Superconductors, Phys. Rev. Lett. **109**, 186802 (2012).
[8] F. Pientka, G. Kells, A. Romito, P. W. Brouwer, and F. von Oppen, Enhanced Zero-Bias Majorana Peak in the Differential Tunneling Conductance of Disordered Multisubband Quantum-Wire/Superconductor Junctions, Phys. Rev. Lett. **109**, 227006 (2012).
[9] D. Bagrets and A. Altland, Class *D* spectral peak in Majorana quantum wires, Phys. Rev. Lett. **109**, 227005 (2012).
[10] J. Liu, A. C. Potter, K. T. Law, and P. A. Lee, Zero-Bias Peaks in the Tunneling Conductance of Spin-Orbit-Coupled Superconducting Wires with and Without Majorana End-States, Phys. Rev. Lett. **109**, 267002 (2012).
[11] D. Rainis, L. Trifunovic, J. Klinovaja, and D. Loss, Towards a realistic transport modeling in a superconducting nanowire with Majorana fermions, Phys. Rev. B **87**, 024515 (2013).
[12] J. D. Sau and S. Das Sarma, Density of states of disordered topological superconductor-semiconductor hybrid nanowires, Phys. Rev. B **88**, 064506 (2013).
[13] R. Žitko, J. S. Lim, R. López, and R. Aguado, Shiba states and zero-bias anomalies in the hybrid normal-superconductor Anderson model, Phys. Rev. B **91**, 045441 (2015).
[14] V. Mourik, K. Zuo, S. Frolov, S. Plissard, E. Bakkers, and L. Kouwenhoven, Signatures of Majorana fermions in hybrid superconductor-semiconductor nanowire devices, Science **336**, 1003 (2012).
[15] M. T. Deng, C. L. Yu, G. Y. Huang, M. Larsson, P. Caroff, and H. Q. Xu, Anomalous zero-bias conductance peak in a Nb-InSb-Nb hybrid device, Nano Lett. **12**, 6414 (2012).
[16] A. Das, Y. Ronen, Y. Most, Y. Oreg, M. Heiblum, and H. Shtrikman, Zero-bias peaks and splitting in an Al-InAs nanowire topological superconductor as a signature of Majorana fermions, Nat. Phys. **8**, 887 (2012).
[17] A. D. K. Finck, D. J. Van Harlingen, P. K. Mohseni, K. Jung, and X. Li, Anomalous Modulation of a Zero-Bias Peak in a Hybrid Nanowire-Superconductor Device, Phys. Rev. Lett. **110**, 126406 (2013).
[18] H. O. H. Churchill, V. Fatemi, K. Grove-Rasmussen, M. T. Deng, P. Caroff, H. Q. Xu, and C. M. Marcus, Superconductornanowire devices from tunneling to the multichannel regime: Zero-bias oscillations and magnetoconductance crossover, Phys. Rev. B **87**, 241401(R) (2013).
[19] E. J. H. Lee, X. Jiang, M. Houzet, R. Aguado, C. M. Lieber, and S. De Franceschi, Spin-resolved Andreev levels and parity crossings in hybrid superconductor–semiconductor nanostructures, Nat. Nanotechnol. **9**, 79 (2014).
[20] W. Chang, S. M. Albrecht, T. S. Jespersen, F. Kuemmeth, P. Krogstrup, J. Nygård, and C. M. Marcus, Hard gap in epitaxial semiconductor-superconductor nanowires, Nat. Nanotechnol. **10**, 232 (2015).
[21] A. P. Higginbotham, S. M. Albrecht, G. Kirsanskas, W. Chang, F. Kuemmeth, P. Krogstrup, T. S. J. J. Nygård, K. Flensberg, and C. M. Marcus, Parity lifetime of bound states in a proximitized semiconductor nanowire, Nat. Phys. **11**, 1017 (2015).
[22] P. Krogstrup, N. L. B. Ziino, W. Chang, S. M. Albrecht, M. H. Madsen, E. Johnson, J. Nygård, C. M. Marcus, and T. S. Jespersen, Epitaxy of semiconductor-superconductor nanowires, Nat. Mater. **14**, 400 (2015).
[23] H. Zhang, Ö. Gül, S. Conesa-Boj, K. Zuo, V. Mourik, F. K. de Vries, J. van Veen, D. J. van Woerkom, M. P. Nowak, M. Wimmer, D. Car, S. Plissard, E. P. A. M. Bakkers, M. Quintero-Pérez, S. Goswami, K. Watanabe, T. Taniguchi, and L. P. Kouwenhoven, Ballistic superconductivity in semiconductor nanowires, Nat. Commun. **8**, 16025 (2017).
[24] S. M. Albrecht, A. P. Higginbotham, M. Madsen, F. Kuemmeth, T. S. Jespersen, J. Nygård, P. Krogstrup, and C. M. Marcus, Exponential protection of zero

modes in Majorana islands, Nature (London) **531**, 206 (2016).
[25] M. T. Deng, S. Vaitiekėnas, E. B. Hansen, J. Danon, M. Leijnse, K. Flensberg, J. Nygård, P. Krogstrup, and C. M. Marcus, Majorana bound state in a coupled quantum-dot hybrid-nanowire system, Science **354**, 1557 (2016).
[26] F. Nichele, A. C. C. Drachmann, A. M. Whiticar, E. C. T. O'Farrell, H. J. Suominen, A. Fornieri, T. Wang, G. C. Gardner, C. Thomas, A. T. Hatke, P. Krogstrup, M. J. Manfra, K. Flensberg, and C. M. Marcus, Scaling of Majorana Zero-Bias Conductance Peaks, Phys. Rev. Lett. **119**, 136803 (2017).
[27] H. J. Suominen, M. Kjaergaard, A. R. Hamilton, J. Shabani, C. J. Palmstrøm, C. M. Marcus, and F. Nichele, Zero-Energy Modes from Coalescing Andreev States in a Two-Dimensional Semiconductor-Superconductor Hybrid Platform, Phys. Rev. Lett. **119**, 176805 (2017).
[28] J. Chen, P. Yu, J. Stenger, M. Hocevar, D. Car, S. R. Plissard, E. P. A. M. Bakkers, T. D. Stanescu, and S. M. Frolov, Experimental phase diagram of zero-bias conductance peaks in superconductor/semiconductor nanowire devices, Sci. Adv. **3**, e1701476 (2017).
[29] M.-T. Deng, S. Vaitiekėnas, E. Prada, P. San-Jose, J. Nygård, P. Krogstrup, R. Aguado, and C. M. Marcus, Nonlocality of Majorana modes in hybrid nanowires, Phys. Rev. B **98**, 085125 (2018).
[30] H. Zhang *et al.*, Quantized Majorana conductance, Nature (London) **556**, 74 (2018).
[31] E. Prada, P. San-Jose, and R. Aguado, Transport spectroscopy of NS nanowire junctions with Majorana fermions, Phys. Rev. B **86**, 180503(R) (2012).
[32] J. Cayao, E. Prada, P. San-José, and R. Aguado, SNS junctions in nanowires with spin-orbit coupling: Role of confinement and helicity on the subgap spectrum, Phys. Rev. B **91**, 024514 (2015).
[33] P. San-José, J. Cayao, E. Prada, and R. Aguado, Majorana bound states from exceptional points in non-topological superconductors, Sci. Rep. **6**, 21427 (2016).
[34] C. Fleckenstein, F. Domínguez, N. Traverso Ziani, and B. Trauzettel, Decaying spectral oscillations in a Majorana wire with finite coherence length, Phys. Rev. B **97**, 155425 (2018).
[35] C.-X. Liu, J. D. Sau, T. D. Stanescu, and S. Das Sarma, Andreev bound states versus Majorana bound states in quantum dot-nanowire-superconductor hybrid structures: Trivial versus topological zero-bias conductance peaks, Phys. Rev. B **96**, 075161 (2017).
[36] A. Vuik, B. Nijholt, A. Akhmerov, and M. Wimmer, Reproducing topological properties with quasi-Majorana states, arXiv:1806.02801.
[37] K. T. Law, P. A. Lee, and T. K. Ng, Majorana Fermion Induced Resonant Andreev Reflection, Phys. Rev. Lett. **103**, 237001 (2009).
[38] T. D. Stanescu and S. Das Sarma, Proximity-induced low-energy renormalization in hybrid semiconductor-superconductor Majorana structures, Phys. Rev. B **96**, 014510 (2017).
[39] C. Reeg, D. Loss, and J. Klinovaja, Finite-size effects in a nanowire strongly coupled to a thin superconducting shell, Phys. Rev. B **96**, 125426 (2017).
[40] C. Reeg, D. Loss, and J. Klinovaja, Metallization of a Rashba wire by a superconducting layer in the strong-proximity regime, Phys. Rev. B **97**, 165425 (2018).
[41] C. Reeg, D. Loss, and J. Klinovaja, Proximity effect in a two-dimensional electron gas coupled to a thin superconducting layer, Beilstein J. Nanotechnol. **9**, 1263 (2018).
[42] C. Reeg, O. Dmytruk, D. Chevallier, D. Loss, and J. Klinovaja, Zero-energy Andreev bound states from quantum dots in proximitized Rashba nanowires, Phys. Rev. B **98**, 245407 (2018).
[43] D. E. Liu and H. U. Baranger, Detecting a Majorana-fermion zero mode using a quantum dot, Phys. Rev. B **84**, 201308(R) (2011).
[44] S. Droste, S. Andergassen, and J. Splettstoesser, Josephson current through interacting double quantum dots with spinorbit coupling, J. Phys. Condens. Matter **24**, 415301 (2012).
[45] E. Vernek, P. H. Penteado, A. C. Seridonio, and J. C. Egues, Subtle leakage of a Majorana mode into a quantum dot, Phys. Rev. B **89**, 165314 (2014).
[46] D. A. Ruiz-Tijerina, E. Vernek, L. G. G. V. Dias da Silva, and J. C. Egues, Interaction effects on a Majorana zero mode leaking into a quantum dot, Phys. Rev. B **91**, 115435 (2015).
[47] A. Ptok, A. Kobiałka, and T. Domański, Controlling the bound states in a quantum-dot hybrid nanowire, Phys. Rev. B **96**, 195430 (2017).
[48] C.-X. Liu, J. D. Sau, T. D. Stanescu, and S. Das Sarma, Andreev bound states versus Majorana bound states in quantum dot-nanowire-superconductor hybrid structures: Trivial versus topological zero-bias conductance peaks, Phys. Rev. B **96**, 075161 (2017).
[49] P.-G. de Gennes, *Superconductivity of Metals and Alloys* (Westview Press, Florida, 1999).
[50] A. M. Black-Schaffer and S. Doniach, Self-consistent solution for proximity effect and Josephson current in ballistic graphene SNS Josephson junctions, Phys. Rev. B **78**, 024504 (2008).
[51] K. Björnson, A. V. Balatsky, and A. M. Black-Schaffer, Superconducting order parameter π-phase shift in magnetic impurity wires, Phys. Rev. B **95**, 104521 (2017).
[52] O. A. Awoga, K. Björnson, and A. M. Black-Schaffer, Disorder robustness and protection of Majorana bound states in ferromagnetic chains on conventional superconductors, Phys. Rev. B **95**, 184511 (2017).
[53] A. Theiler, K. Björnson, and A. M. Black-Schaffer, Majorana bound state localization and energy oscillations for magnetic impurity chains on conventional superconductors, arXiv:1808.10061.
[54] M. Mashkoori and A. Black-Schaffer, Majorana bound states in magnetic impurity chains: Effects of *d*-wave pairing, Phys. Rev. B **99**, 024505 (2019).
[55] See Supplemental Material at http://link.aps.org/supplemental/10.1103/PhysRevLett.123.117001 for additional discussions and figures to support the conclusions.
[56] B. D. Woods, S. Das Sarma, and T. D. Stanescu, Electronic structure of full-shell InAs/Al hybrid semiconductorsuperconductor nanowires: Spin-orbit coupling and topological phase space, Phys. Rev. B **99**, 161118 (2019).
[57] A. Alexandradinata, X. Dai, and B. A. Bernevig, Wilson-loop characterization of inversion-symmetric topological insulators, Phys. Rev. B **89**, 155114 (2014).

[58] M. Lee, J. S. Lim, and R. López, Kondo effect in a quantum dot side-coupled to a topological superconductor, Phys. Rev. B **87**, 241402(R) (2013).
[59] C. Schrade and L. Fu, Andreev or Majorana, Cooper finds out, arXiv:1809.06370.
[60] K. Yavilberg, E. Ginossar, and E. Grosfeld, Differentiating Majorana from Andreev bound states in a superconducting circuit, arXiv:1902.07229.
[61] D. Sticlet, C. Bena, and P. Simon, Spin and Majorana Polarization in Topological Superconducting Wires, Phys. Rev. Lett. **108**, 096802 (2012).
[62] K. Björnson and A. M. Black-Schaffer, Skyrmion spin texture in ferromagnetic semiconductor–superconductor heterostructures, Phys. Rev. B **89**, 134518 (2014).
[63] P. Szumniak, D. Chevallier, D. Loss, and J. Klinovaja, Spin and charge signatures of topological superconductivity in Rashba nanowires, Phys. Rev. B **96**, 041401(R) (2017).
[64] M. Serina, D. Loss, and J. Klinovaja, Boundary spin polarization as a robust signature of a topological phase transition in Majorana nanowires, Phys. Rev. B **98**, 035419 (2018).
[65] J. Cayao, P. San-José, A. M. Black-Schaffer, R. Aguado, and E. Prada, Majorana splitting from critical currents in Josephson junctions, Phys. Rev. B **96**, 205425 (2017).
[66] J. Cayao, A. M. Black-Schaffer, E. Prada, and R. Aguado, Andreev spectrum and supercurrents in nanowire-based SNS junctions containing Majorana bound states, Beilstein J. Nanotechnol. **9**, 1339 (2018).
[67] E. Vecino, A. Martín-Rodero, and A. Levy Yeyati, Josephson current through a correlated quantum level: Andreev states and π junction behavior, Phys. Rev. B **68**, 035105 (2003).
[68] C. Beenakker, Transport Phenomena in Mesoscopic Systems, in *Proceedings of the 14th Taniguchi Symposium, Shima, Japan, 1991* (Springer-Verlag, Berlin, 1992), Vol. 109, p. 235.
[69] A. I. Buzdin, Proximity effects in superconductor-ferromagnet heterostructures, Rev. Mod. Phys. **77**, 935 (2005).
[70] W. Chang, V. E. Manucharyan, T. S. Jespersen, J. Nygård, and C. M. Marcus, Tunneling Spectroscopy of Quasiparticle Bound States in a Spinful Josephson Junction, Phys. Rev. Lett. **110**, 217005 (2013).
[71] T. Yokoyama, M. Eto, and Y. V. Nazarov, Josephson current through semiconductor nanowire with spinorbit interaction in magnetic field, J. Phys. Soc. Jpn. **82**, 054703 (2013).
[72] D. Szombati, S. Nadj-Perge, D. Car, S. Plissard, E. Bakkers, and L. Kouwenhoven, Josephson ϕ_0-junction in nanowire quantum dots, Nat. Phys. **12**, 568 (2016).
[73] K. Zuo, V. Mourik, D. B. Szombati, B. Nijholt, D. J. van Woerkom, A. Geresdi, J. Chen, V. P. Ostroukh, A. R. Akhmerov, S. R. Plissard, D. Car, E. P. A. M. Bakkers, D. I. Pikulin, L. P. Kouwenhoven, and S. M. Frolov, Supercurrent Interference in Few-Mode Nanowire Josephson Junctions, Phys. Rev. Lett. **119**, 187704 (2017).
[74] E. J. H. Lee, X. Jiang, R. Žitko, R. Aguado, C. M. Lieber, and S. De Franceschi, Scaling of subgap excitations in a superconductor-semiconductor nanowire quantum dot, Phys. Rev. B **95**, 180502(R) (2017).
[75] J. Saldaña, R. Žitko, J. Cleuziou, E. Lee, V. Zannier, D. Ercolani, L. Sorba, R. Aguado, and S. De Franceschi, Charge localization and reentrant superconductivity in a quasi-ballistic inas nanowire coupled to superconductors, Sci. Adv. **5**, eaav1235 (2019).